

Study of the process $e^+e^- \rightarrow \pi^+\pi^-\pi^0$ in the energy region \sqrt{s} from 0.98 to 1.38 GeV.

M.N.Achasov*, V.M.Aulchenko, K.I.Beloborodov,
 A.V.Berdugin, A.G.Bogdanchikov, A.V.Bozhenok, A.D.Bukin, D.A.Bukin,
 S.V.Burdin, T.V.Dimova, V.P.Druzhinin, V.B.Golubev, V.N.Ivanchenko,
 A.A.Korol, S.V.Koshuba, I.N.Nesterenko, E.V.Pakhtusova, A.A.Polunin,
 A.A.Salnikov, S.I.Serednyakov, V.V.Shary, Yu.M.Shatunov, V.A.Sidorov,
 Z.K.Silagadze, A.N.Skrinsky, A.G.Skripkin, Yu.V.Usov, A.V.Vasiljev

*Budker Institute of Nuclear Physics,
 Siberian Branch of the Russian Academy of Sciences
 and Novosibirsk State University,
 11 Lavrentyev, Novosibirsk,
 630090, Russia
 (June 9, 2019)*

The cross section of the process $e^+e^- \rightarrow \pi^+\pi^-\pi^0$ was measured in the Spherical Neutral Detector experiment at the VEPP-2M collider in the energy region $\sqrt{s} = 980 \div 1380$ MeV. The measured cross section together with the $e^+e^- \rightarrow \pi^+\pi^-\pi^0$ and $\omega\pi^+\pi^-$ cross sections obtained in other experiments was analyzed in the framework of the generalized vector meson dominance model. It was found that the experimental data can be described by a sum of ω , ϕ mesons and two ω' and ω'' resonances contributions, with masses $m_{\omega'} = 1500 \pm^{41}_{34}$, $m_{\omega''} = 1776 \pm^{33}_{27}$ MeV and widths $\Gamma_{\omega'} = 1200 \pm^{251}_{191}$, $\Gamma_{\omega''} = 510 \pm^{106}_{73}$ MeV. The analysis of the $\pi^+\pi^-$ invariant mass spectra in the energy region \sqrt{s} from 1100 to 1380 MeV has shown that for their description one should take into account the $e^+e^- \rightarrow \omega\pi^0 \rightarrow \pi^+\pi^-\pi^0$ mechanism also. The phase between the amplitudes corresponding to the $e^+e^- \rightarrow \omega\pi$ and $e^+e^- \rightarrow \rho\pi$ intermediate states was measured for the first time. The value of the phase is close to zero and depends on energy.

I. INTRODUCTION

The production cross section of hadrons in the e^+e^- annihilation in the energy region $\sqrt{s} < 1.03$ GeV can be described within the vector meson dominance model (VDM) framework and is determined by the amplitudes of light vector mesons ρ, ω, ϕ transitions into the final states. The light vector mesons are studied rather well. They are quark-antiquark $q\bar{q}$ ($q = u, d, s$) bound states, their masses, widths and main decays were measured with high accuracy¹. The production cross section of hadrons above $\phi(1020)$ resonance ($\sqrt{s} \simeq 1.03\text{--}2$ GeV) cannot be described in the conventional VDM framework (taking into account ρ, ω and ϕ mesons only) and this points out the existence of the states with vector meson quantum numbers $I^G(J^{PC}) = 1^+(1^{--}), 0^-(1^{--})$ and with masses about 1450, 1650 MeV. Parameters of these states are not well established due to the poor accuracy and conflicting experimental data. The nature of these states is not clear either. In some reviews of experimental data they are considered as a mixture of $q\bar{q}$ with 4-quark $qq\bar{q}\bar{q}$ and hybrid $q\bar{q}g$ states²⁻⁵. On the other hand the experimental data do not contradict to hypothesis that these states have $q\bar{q}$ structure and are radial and orbital excitations

*e-mail: achasov@inp.nsk.su, FAX: +7(383-2)34-21-63

of the light vector mesons ρ, ω, ϕ^{6-8} . In this context the main experimental task is the improvement of the cross sections measurement accuracy.

As was already mentioned, in the VDM framework the cross section of the process $e^+e^- \rightarrow \pi^+\pi^-\pi^0$ is determined by the amplitudes of vector mesons V ($V = \omega, \phi, \omega', \dots$) transitions into the final state: $V \rightarrow \pi^+\pi^-\pi^0$. The $\rho\pi$ intermediate state dominates in these transitions [Fig.1(a)]. The other mechanism of $V \rightarrow \pi^+\pi^-\pi^0$ transition is also possible via $\rho - \omega$ mixing: $V \rightarrow \omega\pi^0 \rightarrow \rho^0\pi^0$ ($V = \rho, \rho', \rho''$) [Fig.1(b)]. This effect was predicted in Ref.⁹ and was observed in the SND (Spherical Neutral Detector) experiment for the energy range $\sqrt{s} = 1200$ –1400 MeV¹⁰. Besides the studies of the $e^+e^- \rightarrow \pi^+\pi^-\pi^0$ cross section and $\pi\pi$ invariant mass spectra above ϕ -meson production region provides information about vector mesons excited states and their interference.

The $e^+e^- \rightarrow \pi^+\pi^-\pi^0$ cross section in the energy region above ϕ meson and up to 2200 MeV was studied in several experiments^{11–16}, but no one of them have covered the whole region. The SND studies of this cross section in the range $\sqrt{s} = 1040$ –1380 MeV based on a part of collected data was already reported in Ref.¹⁷. Here we present the results obtained by using the full data sample. The present work includes both the total cross section and the dipion mass spectra studies.

II. EXPERIMENT

The SND detector¹⁸ had been running since 1995 up to 2000 at the VEPP-2M¹⁹ collider in the energy range \sqrt{s} from 360 to 1400 MeV. The detector contains several subsystems. The tracking system includes two cylindrical drift chambers. The three-layer spherical electromagnetic calorimeter is based on NaI(Tl) crystals²⁰. The muon/veto system consists of plastic scintillation counters and two layers of streamer tubes. The calorimeter energy and angular resolutions depend on the photon energy as $\sigma_E/E(\%) = 4.2\%/\sqrt[4]{E}(\text{GeV})$ and $\sigma_{\phi,\theta} = 0.82^\circ/\sqrt{E}(\text{GeV}) \oplus 0.63^\circ$. The tracking system angular resolution is about 0.5° and 2° for azimuthal and polar angles respectively. The energy loss resolution dE/dx in the drift chamber is about 30%. SND was described in details in Ref.¹⁸.

In 1997 and 1999 the SND had collected data in the energy region \sqrt{s} from 1040 to 1380 MeV with integrated luminosity about 9.0 pb^{-1} , also about 130 nb^{-1} was collected at $\sqrt{s} = 980$ MeV. The beam energy was calculated from the magnetic field value in the bending magnets and revolution frequency of the collider. The center of mass energy determination accuracy is about 0.1 MeV and the spread of the beam energy is from 0.2 to 0.4 MeV.

For the luminosity measurements, $e^+e^- \rightarrow e^+e^-$ and $e^+e^- \rightarrow \gamma\gamma$ processes were used. In this work the luminosity measured by using $e^+e^- \rightarrow e^+e^-$ process was used for normalizing. The systematic error of the integrated luminosity determination is estimated to be 2%. Since luminosity measurements by $e^+e^- \rightarrow e^+e^-$ and $e^+e^- \rightarrow \gamma\gamma$ reveal a systematic spread of about 1%, this was added to the statistical error of the luminosity determination in each energy point. The statistical accuracy was better than 1%.

III. DATA ANALYSIS

A. Selection of $e^+e^- \rightarrow \pi^+\pi^-\pi^0$ events

The data analysis and selection criteria used in this work are similar to those described in Ref.^{21,22}. During the experimental runs, the first-level trigger¹⁸ selects

events with energy deposition in the calorimeter more than 180 MeV and with two or more charged particles. During processing of the experimental data the event reconstruction is performed^{18,21}. For further analysis, events containing two or more photons and two charged particles with $|z| < 10$ cm and $r < 1$ cm were selected. Here z is the coordinate of the charged particle production point along the beam axis (the longitudinal size of the interaction region depends on beam energy and varies from 2 to 2.5 cm); r is the distance between the charged particle track and the beam axis in the $r - \phi$ plane. Extra photons in $e^+e^- \rightarrow \pi^+\pi^-\pi^0$ events can appear because of the overlap with the beam background or nuclear interactions of the charged pions in the calorimeter. Under these selection conditions, the background sources are $e^+e^- \rightarrow \pi^+\pi^-\pi^0\pi^0$, $e^+e^-\gamma\gamma$, $\pi^+\pi^-\gamma$, K^+K^- , K_SK_L processes and the beam background. Let us note, that in the energy region above ϕ -meson the process $e^+e^- \rightarrow \pi^+\pi^-\pi^0$ does not dominate, even more, its cross section is several times lower then the cross section of the main background process $e^+e^- \rightarrow \pi^+\pi^-\pi^0\pi^0$.

To suppress the beam background, the following cuts on the angle between the two charged particle tracks ψ and energy deposition of the neutral particles E_{neu} were applied: $\psi > 40^\circ$, $E_{neu} > 100$ MeV.

To reject the background from the $e^+e^- \rightarrow K^+K^-$ process, the following cuts were imposed: $(dE/dx) < 5 \cdot (dE/dx)_{min}$ for each charged particle, $(dE/dx) < 3 \cdot (dE/dx)_{min}$ at least for one of them, and $\Delta\phi > 10^\circ$. Here $\Delta\phi$ is an acollinearity angle in the azimuthal plane and $(dE/dx)_{min}$ is an average energy loss of a minimum ionizing particle. The last cut $|\Delta\phi| > 10^\circ$ also suppresses the $e^+e^- \rightarrow \pi^+\pi^-\gamma$ events.

To suppress the $e^+e^- \rightarrow e^+e^-\gamma\gamma$ events the energy deposition of the charged particles E_{cha} was required to be small enough: $E_{cha} < 0.5 \cdot \sqrt{s}$.

For events left after these cuts, a kinematic fit was performed under the following constraints: the charged particles are considered to be pions, the system has zero total momentum, the total energy is \sqrt{s} , and the photons originate from the $\pi^0 \rightarrow \gamma\gamma$ decays. The value of the likelihood function $\chi^2_{3\pi}$ (Fig.2) is calculated during the fit. In events with more than two photons, extra photons are considered as spurious ones and rejected. To do this, all possible subsets of two photons were inspected and the one, corresponding to the maximum likelihood was selected. After the kinematic fit the following additional cuts were applied: $36^\circ < \theta_\gamma < 144^\circ$, $N_\gamma = 2$, and $\chi^2_{3\pi} < 5$. Here θ_γ is polar angle of one of the photons selected by the reconstruction program as originated from the π^0 -decay, N_γ is the number of detected photons. The angular distributions of particles for the selected events are shown in Fig.3,4,5 and 6 while Fig.7 and Fig.8 demonstrate the photon energy distributions for the same events. The experimental and simulated distributions are in agreement.

B. Background subtraction

The number of background events was estimated by using simulation in the following way:

$$N_{bkg}(s) = \sum_i \sigma_{Ri}(s) \epsilon_i(s) IL(s), \quad (1)$$

where i is a process number, $\sigma_{Ri}(s)$ is the cross section of the background process taking into account the radiative corrections, $IL(s)$ is the integrated luminosity, $\epsilon_i(s)$ is the detection probability for the background process under selection described above. The $e^+e^- \rightarrow \pi^+\pi^-\gamma$ cross section was calculated for the case, when the photon has the energy above 10 MeV and is radiated at the angle θ more than 10° . As it was mentioned above the main source of background are the events of

the $e^+e^- \rightarrow \pi^+\pi^-\pi^0\pi^0$ process. Two mechanisms contribute into the total cross section of this process: $e^+e^- \rightarrow \omega\pi$ and $e^+e^- \rightarrow \rho\pi\pi$. It was shown in Ref.^{23,24} that the $e^+e^- \rightarrow \rho\pi\pi$ process dynamics can be described with the $a_1\pi$ intermediate state. The SND studies of the $e^+e^- \rightarrow \pi^+\pi^-\pi^0\pi^0$ process²⁵ agree with this conclusion. For background estimation the $e^+e^- \rightarrow \omega\pi$ and $e^+e^- \rightarrow \rho\pi\pi$ cross sections measured in SND experiments were used^{25,26}. To obtain the detection probability of the $e^+e^- \rightarrow \rho\pi\pi$ events the simulation with $a_1\pi$ intermediate state was used. The numbers of $e^+e^- \rightarrow \pi^+\pi^-\pi^0(\gamma)$ events (after background subtraction) and background event numbers are shown in Table I. Here γ is a photon emitted by initial particles.

To estimate the accuracy of background events number determination the $\chi^2_{3\pi}$ distribution (Fig.2) was studied. Experimental $\chi^2_{3\pi}$ distribution in the range $0 < \chi^2_{3\pi} < 20$ was fitted by a sum of background and signal. The distribution for background events was taken from the simulation and distribution for $e^+e^- \rightarrow \pi^+\pi^-\pi^0$ events was obtained by using data collected in the vicinity of the ϕ meson peak^{21,22} ($\chi^2_{3\pi}$ distribution actually does not change in the interval $\sqrt{s} = 1 - 1.4$ GeV). As a result the ratio 1.4 ± 0.2 between background events number obtained from the fit and the number calculated according to (1) was found. Using this ratio the accuracy of background events number determination can be estimated to be about 40%.

C. Detection efficiency

The detection efficiency of the $e^+e^- \rightarrow \pi^+\pi^-\pi^0(\gamma)$ process was obtained from simulation. The detection efficiency for the events without γ -quantum radiation depends on the center of mass energy and varies from 0.15 to 0.16 in the energy range $\sqrt{s} = 980 - 1380$ MeV. This dependence can be approximated by a linear function. The detection efficiency dependence on the radiated photon energy is shown in Fig.9.

Inaccuracies in the simulation of the $\chi^2_{3\pi}$, dE/dx , N_γ distributions lead to an error in the average detection efficiency determination. To take into account this uncertainties, the detection efficiency was multiplied by correction coefficients, which were obtained in the following way²¹. The experimental events were selected without any conditions on the parameter under study, using the selection parameters uncorrelated with the studied one. The same selection criteria was applied for simulated events. Then the cut was applied to the parameter and the correction coefficient was calculated:

$$\delta = \frac{n/N}{m/M}, \quad (2)$$

where N and M are the number of events in experiment and simulation respectively selected without any cuts on the parameter under study; n and m are the number of events in experiment and simulation when the cut on the parameter was applied. As a rule, the error in the coefficient δ determination is connected with the uncertainty of background subtraction. This systematic error was estimated by varying other selection criteria. The correction coefficient $\delta_{\chi^2_{3\pi}} = 0.91 \pm 0.03$, due to uncertainty in the $\chi^2_{3\pi}$ distribution simulation, was obtained using data collected in the vicinity of the ϕ resonance^{21,22}. The correction, which takes into account the inaccuracy of extra photons simulation is $\delta_{N_\gamma} = 0.87 \pm 0.02$, and correction due to inaccuracy of dE/dx energy losses simulation is $\delta_{dE/dx} = 0.98 \pm 0.01$. The overlap of the beam background with the events containing charged particles can result in track reconstruction failure and a decrease of detection efficiency. To take into account

this effect, background events (experimental events collected when detector was triggered with an external generator) were overlapped with the simulated events. It was found that the detection efficiency decreased by about 3% and therefore the correction coefficient $\delta_{over} = 0.97 \pm 0.03$ was used.

The total correction used in this work is equal to:

$$\delta_{tot} = \delta_{\chi_{3\pi}^2} \times \delta_{dE/dx} \times \delta_{N_\gamma} \times \delta_{over} = 0.75 \pm 0.04.$$

The systematic error of detection efficiency determination is 5%. The detection efficiency after the applied corrections is shown in Table I.

IV. THEORETICAL FRAMEWORK

In the VDM framework the cross section of the $e^+e^- \rightarrow \pi^+\pi^-\pi^0$ process is

$$\frac{d\sigma}{dm_0 dm_+} = \frac{4\pi\alpha}{s^{3/2}} \frac{|\vec{p}_+ \times \vec{p}_-|^2}{12\pi^2 \sqrt{s}} m_0 m_+ \cdot |F|^2, \quad (3)$$

where \vec{p}_+ and \vec{p}_- are the π^+ and π^- momenta, m_0 and m_+ are $\pi^+\pi^-$ and $\pi^+\pi^0$ invariant masses. Formfactor F of the $\gamma^* \rightarrow \pi^+\pi^-\pi^0$ transition has the form

$$|F|^2 = \left| A_{\rho\pi}(s) \sum_{i=+,0,-} \frac{g_{\rho^i\pi\pi}}{D_\rho(m_i)} + A_{\omega\pi}(s) \frac{\Pi_{\rho\omega} g_{\rho^0\pi\pi}}{D_\rho(m_0) D_\omega(m_0)} \right|^2. \quad (4)$$

Here

$$D_\rho(m_i) = m_{\rho^i}^2 - m_i^2 - im_i \Gamma_{\rho^i}(m_i),$$

$$\Gamma_{\rho^i}(m_i) = \left(\frac{m_{\rho^i}}{m_i} \right)^2 \cdot \Gamma_{\rho^i} \cdot \left(\frac{q_i(m_i)}{q_i(m_{\rho^i})} \right)^3$$

$$q_0(m) = \frac{1}{2} (m^2 - 4m_\pi^2)^{1/2},$$

$$q_\pm(m) = \frac{1}{2m} [(m^2 - (m_{\pi^0} + m_\pi)^2)(m^2 - (m_{\pi^0} - m_\pi)^2)]^{1/2}$$

$$m_- = \sqrt{s + m_{\pi^0}^2 + 2m_\pi^2 - m_0^2 - m_+^2},$$

where m_- is the $\pi^-\pi^0$ invariant mass, m_{π^0} and m_π are the neutral and charged pion masses, i denotes the sign of a ρ -meson ($\pi\pi$ pair) charge. The $\rho^0 \rightarrow \pi^+\pi^-$ and $\rho^\pm \rightarrow \pi^\pm\pi^0$ transition coupling constants could be determined in the following way:

$$g_{\rho^0\pi\pi}^2 = \frac{6\pi m_{\rho^0}^2 \Gamma_{\rho^0}}{q_0(m_{\rho^0})^3},$$

$$g_{\rho^\pm\pi\pi}^2 = \frac{6\pi m_{\rho^\pm}^2 \Gamma_{\rho^\pm}}{q_\pm(m_{\rho^\pm})^3}$$

Experimental data²² do not contradict to the equality of the coupling constants $g_{\rho^0\pi\pi}^2 = g_{\rho^\pm\pi\pi}^2$. In this case the ρ^0 and ρ^\pm meson widths are related as follows:

$$\Gamma_{\rho^\pm} = \Gamma_{\rho^0} \frac{m_{\rho^0}^2}{m_{\rho^\pm}^2} \frac{q_\pm(m_{\rho^\pm})^3}{q_0(m_{\rho^0})^3}. \quad (5)$$

In the subsequent analysis we assume that $g_{\rho^0\pi\pi}^2 = g_{\rho^\pm\pi\pi}^2$, and the width values were taken from SND measurements²² $\Gamma_{\rho^0} = 149.8$ MeV, $\Gamma_{\rho^\pm} = 150.9$ MeV. The neutral and charged ρ mesons masses were assumed to be equal and also were taken from the SND measurements²² $m_\rho = 775.0$ MeV.

The second term in (4) takes into account the $\rho - \omega$ mixing⁹. The polarization operator of this mixing $\Pi_{\rho\omega}$ satisfies $\text{Im}(\Pi_{\rho\omega}) \ll \text{Re}(\Pi_{\rho\omega})$ ^{27,28}, where

$$\text{Re}(\Pi_{\rho\omega}) = \sqrt{\frac{\Gamma_\omega}{\Gamma_{\rho^0}(m_\omega)}} B(\omega \rightarrow \pi^+ \pi^-) \cdot \left| (m_\omega^2 - m_\rho^2) - im_\omega(\Gamma_\omega - \Gamma_{\rho^0}(m_\omega)) \right|, \quad (6)$$

So we have assumed $\text{Im}(\Pi_{\rho\omega}) = 0$ in the subsequent analysis.

The $e^+e^- \rightarrow \pi^+ \pi^- \pi^0$ process cross section can be written in the following way:

$$\sigma_{3\pi} = \sigma_{\rho\pi \rightarrow 3\pi} + \sigma_{\omega\pi \rightarrow 3\pi} + \sigma_{int}, \quad (7)$$

where

$$\sigma_{\rho\pi \rightarrow 3\pi} = \frac{4\pi\alpha}{s^{3/2}} W_{\rho\pi}(s) \left| A_{\rho\pi}(s) \right|^2, \quad (8)$$

$$\sigma_{\omega\pi \rightarrow 3\pi} = \frac{4\pi\alpha}{s^{3/2}} W_{\omega\pi}(s) \left| A_{\omega\pi}(s) \right|^2, \quad (9)$$

$$\sigma_{int} = \frac{4\pi\alpha}{s^{3/2}} \left\{ A_{\rho\pi}(s) A_{\omega\pi}^*(s) W_{int}(s) + A_{\rho\pi}^*(s) A_{\omega\pi}(s) W_{int}^*(s) \right\}. \quad (10)$$

The phase space factors $W_{\rho\pi}(s)$, $W_{\omega\pi}(s)$ and $W_{int}(s)$ were calculated as follows:

$$W_{\rho\pi}(s) = \frac{1}{12\pi^2 \sqrt{s}} \int_{2m_\pi}^{\sqrt{s}-m_{\pi^0}} m_0 dm_0 \int_{m_+^{min}(m_0)}^{m_+^{max}(m_0)} m_+ dm_+ |\vec{p}_+ \times \vec{p}_-|^2 \cdot \left| \sum_{i=+,0,-} \frac{g_{\rho^i\pi\pi}}{D_\rho(m_i)} \right|^2, \quad (11)$$

$$W_{\omega\pi}(s) = \frac{1}{12\pi^2 \sqrt{s}} \int_{2m_\pi}^{\sqrt{s}-m_{\pi^0}} m_0 dm_0 \int_{m_+^{min}(m_0)}^{m_+^{max}(m_0)} m_+ dm_+ |\vec{p}_+ \times \vec{p}_-|^2 \cdot \left| \frac{\Pi_{\rho\omega} g_{\rho^0\pi\pi}}{D_\rho(m_0) D_\omega(m_0)} \right|^2, \quad (12)$$

$$W_{int}(s) = \frac{1}{12\pi^2 \sqrt{s}} \int_{2m_\pi}^{\sqrt{s}-m_{\pi^0}} m_0 dm_0 \int_{m_+^{min}(m_0)}^{m_+^{max}(m_0)} m_+ dm_+ |\vec{p}_+ \times \vec{p}_-|^2 \cdot \left(\left[\frac{\Pi_{\rho\omega} g_{\rho^0\pi\pi}}{D_\rho(m_0) D_\omega(m_0)} \right]^* \cdot \sum_{i=+,0,-} \frac{g_{\rho^i\pi\pi}}{D_\rho(m_i)} \right), \quad (13)$$

Amplitudes of the $\gamma^* \rightarrow \rho\pi$ and $\gamma^* \rightarrow \omega\pi^0$ transitions have the form

$$A_{\rho\pi}(s) = \sum_{V=\omega, \phi, \omega', \dots} \frac{g_{\gamma V} g_{V\rho\pi}}{D_V(s)} e^{i\phi_{\omega V}}, \quad (14)$$

$$A_{\omega\pi}(s) = \sum_{V=\rho, \rho', \dots} \frac{g_{\gamma V} g_{V\omega\pi^0}}{D_V(s)} e^{i\phi_{\rho V}}, \quad (15)$$

where

$$D_V(s) = m_V^2 - s - i\sqrt{s}\Gamma_V(s), \quad \Gamma_V(s) = \sum_f \Gamma(V \rightarrow f, s).$$

Here f denotes the final state of the vector meson V decay. The $\phi_{\omega V}$ ($\phi_{\rho V}$) are relative interference phases between vector mesons V and ω (ρ), so $\phi_{\omega\omega} = 0$ and $\phi_{\rho\rho} = 0$. The coupling constants are determined through the decay branching ratios in the following way:

$$|g_{V\gamma}| = \left[\frac{3m_V^3 \Gamma_V B(V \rightarrow e^+ e^-)}{4\pi\alpha} \right]^{1/2} \quad (16)$$

$$|g_{V\rho\pi}| = \left[\frac{4\pi\Gamma_V B(V \rightarrow \rho\pi)}{W_{\rho\pi}(m_V)} \right]^{1/2}, \quad (17)$$

$$|g_{V\omega\pi}| = \left[\frac{12\pi\Gamma_V B(V \rightarrow \omega\pi)}{q_{\omega\pi}^3(m_V)} \right]^{1/2}, \quad (18)$$

where $q_{\omega\pi}(s)$ is the ω -meson momentum.

V. CROSS SECTION MEASUREMENT

Using data from Table I the $e^+e^- \rightarrow \pi^+\pi^-\pi^0(\gamma)$ process cross section can be calculated as follows:

$$\sigma(s) = \frac{N_{3\pi}(s)}{IL(s)\xi(s)}, \quad (19)$$

where $N_{3\pi}(s)$ is the number of selected $e^+e^- \rightarrow \pi^+\pi^-\pi^0(\gamma)$ events, $IL(s)$ is the integrated luminosity, $\xi(s)$ is the function which takes into account the detection efficiency and radiative corrections:

$$\xi(s) = \frac{\int_0^{E_\gamma^{max}} \sigma_{3\pi}(s, E_\gamma) F(s, E_\gamma) \epsilon(s, E_\gamma) dE_\gamma}{\sigma_{3\pi}(s)}. \quad (20)$$

Here E_γ is the emitted photon energy, $F(s, E_\gamma)$ is the electron ‘‘radiator’’ function²⁹, $\epsilon(s, E_\gamma)$ is the detection efficiency of the process $e^+e^- \rightarrow \pi^+\pi^-\pi^0(\gamma_{rad})$ in dependence from the emitted photon energy and the energy in the e^+e^- center of mass system, $\sigma_{3\pi}(s)$ is the theoretical dependence of the cross section on energy given by equation (7).

To obtain the values of $\xi(s)$ in each energy point the visible cross section of the process $e^+e^- \rightarrow \pi^+\pi^-\pi^0(\gamma_{rad})$

$$\sigma^{vis}(s) = \frac{N_{3\pi}(s)}{IL(s)}$$

was fitted by theoretical energy dependence

$$\sigma^{th}(s) = \sigma_{3\pi}(s)\xi(s).$$

The following logarithmic likelihood function was minimized:

$$\chi^2 = \sum_i \frac{(\sigma_i^{vis} - \sigma_i^{th})^2}{\sigma_i^2},$$

where i is the energy point number, σ_i is the error of the visible cross section σ^{vis} .

In a good approximation the contributions $\sigma_{\omega\pi \rightarrow 3\pi}$ and σ_{int} in expression (7) can be omitted, as they are rather small ($\sim 5 - 10 \%$) and actually does not modify the shape of $\sigma_{3\pi}(s)$ energy dependence. So we assumed that $\sigma_{3\pi}(s) = \sigma_{\rho\pi \rightarrow 3\pi}(s)$. Amplitude of the $\gamma^* \rightarrow \rho\pi$ transition (14) was written as

$$A_{\rho\pi}(s) = \frac{1}{\sqrt{4\pi\alpha}} \sum_{V=\omega,\phi,\omega',\omega''} \frac{\Gamma_V m_V^2 \sqrt{m_V \sigma(V \rightarrow 3\pi)}}{D_V(s)} \frac{e^{i\phi_{\omega V}}}{\sqrt{W_{\rho\pi}(m_V)}}, \quad (21)$$

where

$$\sigma(V \rightarrow X) = \frac{12\pi B(V \rightarrow e^+e^-)B(V \rightarrow X)}{m_V^2}.$$

The following form of the ω' and ω'' total width energy dependence was used

$$\Gamma_V(s) = \Gamma_V \frac{W_{\rho\pi}(s)}{W_{\rho\pi}(m_V)}.$$

In the fit the ω meson parameters (mass, width, main decays branching ratios) were fixed at their PDG values¹, and the ϕ meson mass and width were fixed at the values measured by SND²¹. It was shown²¹, that the $\sigma(\phi \rightarrow 3\pi)$ parameter has a rather large model inaccuracy (about 3%), due to the uncertainty in choice of the phase $\phi_{\omega\phi}$ and the value of additional, besides the ϕ and ω resonances, contributions to the transition amplitude. Therefore we have taken the $\sigma(\phi \rightarrow 3\pi)$ as a free parameter in the fit and the data presented in this work were fitted together with the data from Ref.²¹. The masses and width of ω' , ω'' resonances were free parameters of the fit. Phases $\phi_{\omega V}$ can deviate from 180° or 0° and their values can have energy dependence due to mixing between vector mesons. For example, phase $\phi_{\omega\phi}$ was found to be close to 180° ²¹ and agree with prediction³⁰ $\phi_{\omega\phi} = \Phi(s)$ ($\Phi(m_\phi) \simeq 163^\circ$), where the function $\Phi(s)$ is defined in Ref.³⁰. There are no theoretical predictions about $\phi_{\omega\omega'}$ and $\phi_{\omega\omega''}$ values and their energy dependences, and we have considered $\sqrt{\sigma(\omega' \rightarrow 3\pi)}$ and $\sqrt{\sigma(\omega'' \rightarrow 3\pi)}$ as free parameters, i.e. $\phi_{\omega\omega'}$ and $\phi_{\omega\omega''}$ can be equal to 0 or 180 degrees. The $\xi(s)$ values were obtained by approximation of the experimental data in several models:

1. $\phi_{\omega\phi} = 180^\circ$
2. $\phi_{\omega\phi} = \Phi(s)$
3. $\phi_{\omega\phi}$ is a free parameter

4. $\sigma(\omega'' \rightarrow 3\pi) = 0, \phi_{\omega\phi} = 180^\circ$
5. $\sigma(\omega'' \rightarrow 3\pi) = 0, \phi_{\omega\phi} = \Phi(s)$
6. $\sigma(\omega'' \rightarrow 3\pi) = 0, \phi_{\omega\phi}$ is a free parameter.

The values of $\xi(s)$ significantly depend on the applied model in the energy range $\sqrt{s} \simeq 1040 - 1090$ MeV, and at $\sqrt{s} = 1040$ MeV the $\xi(s)$ values are differ by a factor 10 for different models. Above 1090 MeV the $\xi(s)$ model dependence is negligible. Using obtained $\xi(s)$ values the cross section of the $e^+e^- \rightarrow \pi^+\pi^-\pi^0$ process was calculated (Table.II). The systematic error of the cross section determination in each energy point \sqrt{s} is equal to

$$\sigma_{sys} = \sigma_{eff} \oplus \sigma_{IL} \oplus \sigma_{mod}(s) \oplus \sigma_{bkg}(s).$$

Here $\sigma_{eff} = 5\%$ and $\sigma_{IL} = 2\%$ are systematic uncertainties in detection efficiency and integrated luminosity, which are common for all energy points. The model uncertainty $\sigma_{mod}(s)$ is significant in the region $\sqrt{s} = 1027 - 1080$ MeV and was obtained from the difference of $\xi(s)$ values determined for the six models mentioned above. The error $\sigma_{bkg}(s)$ takes into account the inaccuracy ($\sim 40\%$) of background subtraction and depends on the beam energy.

The obtained cross section differs by about $30 \pm 15\%$ from previous SND result¹⁷ (Fig.10), which claimed systematic error about 12%. This difference can be attributed to the fact that in the new analysis we implemented some corrections to the detection efficiency which were not used in the previous one. The comparison of the measured cross section with the other experimental results is presented in Fig.11.

VI. APPROXIMATION OF THE $\pi^+\pi^-$ MASS SPECTRA.

The contribution of the $e^+e^- \rightarrow \omega\pi^0 \rightarrow \rho^0\pi^0 \rightarrow \pi^+\pi^-\pi^0$ mechanism to the process $e^+e^- \rightarrow \pi^+\pi^-\pi^0$ is seen as the interference in the $\pi^+\pi^-$ invariant mass spectra. To analyze the dipion mass spectra, the formfactor F (expression (4)) was presented in the following form:

$$|F|^2 = \left| A_{\rho\pi}(s) \right|^2 \times \left| \sum_{i=+,0,-} \frac{g_{\rho^i\pi\pi}}{D_\rho(m_i)} + R(s) e^{i\psi(s)} \frac{\text{Re}(\Pi_{\rho\omega}) g_{\rho^0\pi\pi}}{D_\rho(m_0) D_\omega(m_0)} \right|^2, \quad (22)$$

where $R(s)$ is the absolute value, and $\psi(s)$ is the phase of the ratio $A_{\omega\pi}(s)/A_{\rho\pi}(s)$. The $\psi(s)$ energy dependence can be obtained from the approximation of the experimental $\pi^+\pi^-$ invariant mass spectra as described below. The $R(s)$ value was calculated from the equation

$$R^2 \cdot \left(W_{\omega\pi}(s) - \frac{q_{\omega\pi}^3(s)}{3} \frac{\sigma_{3\pi}(s)}{\sigma_{\omega\pi}(s)} \right) + R \cdot \left(e^{-i\psi} W_{int}(s) + e^{i\psi} W_{int}^*(s) \right) + W_{\rho\pi}(s) = 0, \quad (23)$$

which follows from expressions (8-10). The $e^+e^- \rightarrow \omega\pi^0$ cross section was obtained from SND measurements of the $e^+e^- \rightarrow \omega\pi^0 \rightarrow \pi^0\pi^0\gamma$ cross section²⁶: $\sigma_{\omega\pi^0} = \sigma_{\omega\pi^0 \rightarrow \pi^0\pi^0\gamma}/B(\omega \rightarrow \pi^0\gamma)$, $\sigma_{3\pi}(s)$ is the $e^+e^- \rightarrow \pi^+\pi^-\pi^0$ cross section measured here (Table II).

The real part of the polarization operator $\Pi_{\rho\omega}$ is proportional to $\sqrt{B(\omega \rightarrow \pi^+\pi^-)}$. The world average value for this branching ratio is $B(\omega \rightarrow \pi^+\pi^-) = 2.21 \pm 0.30\%$. The results of $B(\omega \rightarrow \pi^+\pi^-)$ measurements in different experiments deviate from

each other by a factor more than 1.5. For example, OLYA detector reported the value $B(\omega \rightarrow \pi^+ \pi^-) = 2.3 \pm 0.5\%$ ³¹, while CMD-2 experiment reported $B(\omega \rightarrow \pi^+ \pi^-) = 1.33 \pm 0.25\%$ ³². So $B(\omega \rightarrow \pi^+ \pi^-)$ was considered as a free parameter of the fit.

For the mass spectra analysis the events selected in the energy region $\sqrt{s} \geq 1100$ MeV were used. For each energy point the $\pi^+ \pi^-$ mass spectra were formed and arranged in histograms with a dipion mass range from 280 to 1240 MeV and bin width of 40 MeV. The invariant mass values were calculated after the kinematic reconstruction. The expected background was subtracted bin by bin while forming the desired histograms.

The dipion mass spectra analysis was performed in the way similar to those described in Ref.²². The experimental spectra were fitted with theoretical distributions. Using the $e^+ e^- \rightarrow \pi^+ \pi^- \pi^0$ cross section (3) and formfactor (22), the theoretical spectra were calculated in the following way:

$$S_j^{(0)}(s) = \frac{1}{C_S(s)} \cdot \int_{m_j - \Delta}^{m_j + \Delta} m_0 dm_0 \int_{m_+^{min}(m_0)}^{m_+^{max}(m_0)} m_+ dm_+ |\vec{p}_+ \times \vec{p}_-|^2 \cdot |F|^2, \quad (24)$$

where j is the bin number, $\Delta = 20$ MeV - half of the bin width, m_j - the central value of the invariant mass in the j th bin, $C_S(s)$ - normalizing coefficient. These spectra were corrected taking into account the detection efficiency $\epsilon_j^{(0)}$ for the j th bin and a probability $a_{ij}^{(0)}$ for the event belonging to the j th bin to migrate to the i th bin due to finite detector resolution

$$G_i^{(0)}(s) = \frac{1}{C_G(s)} \left(\sum_j a_{ij}^{(0)} S_j^{(0)}(s) \epsilon_j^{(0)} \right) \cdot (1 + \delta_i^{(0)}(s)). \quad (25)$$

Here $\delta_i^{(0)}(s)$ is a radiative correction and $C_G(s)$ - normalizing coefficient. The values of $a_{ij}^{(0)}$, $\epsilon_j^{(0)}$ and $\delta_i^{(0)}(s)$ were obtained from simulation.

The function to be minimized was

$$\chi^2 = \sum_s \chi_0^2(s) = \sum_s \sum_i \left(\frac{H_i^{(0)} - G_i^{(0)}}{\sigma_i^{(0)}} \right)^2. \quad (26)$$

Here $H^{(0)}$ is the normalized experimental $\pi^+ \pi^-$ mass distribution (histogram); $\sigma_i^{(0)} = \Delta H_i^{(0)} \oplus \Delta G_i^{(0)}$ include the uncertainties $\Delta H_i^{(0)}$ and $\Delta G_i^{(0)}$ of the experimental and theoretical distributions ($\Delta H_i^{(0)} \gg \Delta G_i^{(0)}$).

During the fitting the phase $\psi(s)$ at each energy point and $B(\omega \rightarrow \pi^+ \pi^-)$ were free parameters. Values of the phase $\psi(s)$ were allowed to vary from -180° to 180° . The obtained $\psi(s)$ values are presented in Table III. The systematic inaccuracy of $\psi(s)$ is about 7° and is connected with systematic error in $R(s)$ determination, which in its turn is about 4% due to uncertainties of $\sigma_{\omega\pi}$ and $\sigma_{3\pi}$ measurements. The $\omega \rightarrow \pi^+ \pi^-$ decay probability was found to be equal to $2.38 \pm_{0.90}^{1.77} \pm 0.18\%$, where systematic error is connected also with the uncertainty of the $R(s)$ ratio determination. In the Fig.12 and 13 the experimental $\pi\pi$ mass spectra together with the theoretical distributions obtained from the fit and the spectra expected from the only $\rho\pi$ intermediate state model are shown. In the $\pi^+ \pi^-$ mass spectra the peak in the ω meson region is clearly seen. The distribution of the invariant mass of the $\pi^\pm \pi^0$ pairs does not contradict to the $\rho\pi$ intermediate state model at the level of our statistical accuracy. These figures demonstrate that together with the $\rho\pi$ intermediate state the $\omega\pi^0$ intermediate state also contributes into the process $e^+ e^- \rightarrow \pi^+ \pi^- \pi^0$.

VII. THE $e^+e^- \rightarrow \pi^+\pi^-\pi^0$ TOTAL CROSS SECTION ANALYSIS.

The analysis of the $e^+e^- \rightarrow \pi^+\pi^-\pi^0$ cross section energy dependence obtained here (Table II) meet the following difficulties:

1. The cross section was measured in the limited \sqrt{s} energy region and it is necessary to use the results of other experiments, while relative systematic error of the measurements is, in general, unknown;
2. In ideal case, to obtain the vector mesons parameters, the combined fit of all $e^+e^- \rightarrow \text{hadrons}$ cross sections is necessary;

The cross section measured in this work was analyzed together with the DM2 results of the $e^+e^- \rightarrow \pi^+\pi^-\pi^0$ and $\omega\pi^+\pi^-$ ¹⁶ cross sections measurements. In addition the preliminary SND results on the $e^+e^- \rightarrow \omega\pi^+\pi^-$ cross section³³ were used. This preliminary data agree with CMD2 results reported in Ref.³⁴. The $e^+e^- \rightarrow \pi^+\pi^-\pi^0$ cross section was fitted by the expression (7). The $A_{\rho\pi}$ amplitude was written in the following way:

$$A_{\rho\pi}(s) = \frac{1}{\sqrt{4\pi\alpha}} \left(\frac{\Gamma_\omega m_\omega^2 \sqrt{m_\omega \sigma(\omega \rightarrow 3\pi)}}{D_\omega(s)} \frac{1}{\sqrt{W_{\rho\pi}(m_\omega)}} + \frac{\Gamma_\phi m_\phi^2 \sqrt{m_\phi \sigma(\phi \rightarrow 3\pi)}}{D_\phi(s)} \frac{e^{i\Phi(s)}}{\sqrt{W_{\rho\pi}(m_\phi)}} + \sum_{i=1}^3 \frac{\Gamma_{\omega^i} m_{\omega^i}^2 \sqrt{m_{\omega^i} \sigma(\omega^i \rightarrow 3\pi)}}{D_{\omega^i}(s)} \frac{e^{i\phi_{\omega\omega^i}}}{\sqrt{W_{\rho\pi}(m_{\omega^i})}} \right), \quad (27)$$

where i is the resonance number. The following form of the energy dependence of the ω^i total widths was used:

$$\Gamma_{\omega^1}(s) = \Gamma_{\omega^1} \frac{W_{\rho\pi}(s)}{W_{\rho\pi}(m_{\omega^1})}, \quad (28)$$

$$\Gamma_{\omega^i}(s) = \Gamma_{\omega^i} \left(B(\omega^i \rightarrow 3\pi) \frac{W_{\rho\pi}(s)}{W_{\rho\pi}(m_{\omega^i})} + B(\omega^i \rightarrow \omega\pi\pi) \frac{W_{\omega\pi\pi}(s)}{W_{\omega\pi\pi}(m_{\omega^i})} \right), \quad i = 2, 3. \quad (29)$$

Here $W_{\omega\pi\pi}(s)$ is the phase space factor of the $\omega\pi\pi$ final state⁷. The probabilities of the ω^i decays into $\pi^+\pi^-\pi^0$ and $\omega\pi\pi$ were calculated in the following way:

$$B(\omega^i \rightarrow f) = \frac{\sigma(\omega^i \rightarrow f)}{\sum_f \sigma(\omega^i \rightarrow f)}. \quad (30)$$

Here $\sigma(\omega^i \rightarrow \omega\pi\pi) = 1.5 \cdot \sigma(\omega^i \rightarrow \omega\pi^+\pi^-)$. In the total width energy dependence the contributions from the following final states were neglected: $K_SK^\pm\pi^\mp$, $K^{*0}K^-\pi^+$, $\bar{K}^{*0}K^+\pi^-$, $K\bar{K}$. The ω meson parameters were fixed according to the PDG table values¹. The m_ϕ , Γ_ϕ and parameters of the $\phi \rightarrow K\bar{K}$ and $\eta\gamma$ decays were fixed at the values obtained by SND²¹, while $\sigma(\phi \rightarrow 3\pi)$ was a free parameter of the fit. As it was mentioned, above the phases $\phi_{\omega\omega^i}$ can differ from 0 or 180 degrees and have the energy dependence. Here we consider only the $\sqrt{\sigma(\omega^i \rightarrow 3\pi)}$ as free parameter, i.e. $\phi_{\omega\omega^i} = 0^\circ$ or 180° .

For the $A_{\omega\pi}$ amplitude two models with different energy behavior of the phase were used. Their parameters were obtained by fitting of the $e^+e^- \rightarrow \omega\pi^0 \rightarrow \pi^0\pi^0\gamma$ cross section measured by SND²⁶ and CLEO2 data on $\tau \rightarrow 3\pi\pi^0$ decay³⁶ (Fig.14). The first model was suggested in Ref.²⁶. It assumes that into the $e^+e^- \rightarrow \omega\pi$ cross section only the ρ and ρ'' resonances contribute (i.e. $A_{\omega\pi} = A_{\rho \rightarrow \omega\pi} + A_{\rho'' \rightarrow \omega\pi}$), at that the following parameters are used: the coupling constant $g_{\rho\omega\pi} \sim$

15.2 GeV^{-1} , ρ'' -mass $m_{\rho''} \sim 1700$ MeV, width $\Gamma_{\rho''} \sim 1$ GeV, phase $\phi_{\rho\rho''} = 180^\circ$ and $\sigma(\rho'' \rightarrow \omega\pi) \sim 9$ nb. The ρ'' total width energy dependence is taken to be the following

$$\Gamma_{\rho''}(s) = \Gamma_{\rho''} \left(0.1 \frac{m_{\rho''}^2}{s} \frac{q_{\pi\pi}^3(s)}{q_{\pi\pi}^3(m_{\rho''})} + 0.9 \frac{q_{\omega\pi}^3(s)}{q_{\omega\pi}^3(m_{\rho''})} \right), \quad (31)$$

where $q_{\pi\pi}(s)$ is the pion momentum. The second model assumes that into the $e^+e^- \rightarrow \omega\pi$ cross section the three ρ , ρ' and ρ'' resonances contribute (i.e. $A_{\omega\pi} = A_{\rho \rightarrow \omega\pi} + A_{\rho' \rightarrow \omega\pi} + A_{\rho'' \rightarrow \omega\pi}$). In this case the parameters of the model are: $g_{\rho\omega\pi} \sim 16.8$ GeV^{-1} , $m_{\rho'} \sim 1480$ MeV, $\Gamma_{\rho'} \sim 790$ MeV, $\phi_{\rho\rho'} = 180^\circ$, $\sigma(\rho' \rightarrow \omega\pi) \sim 86$ nb, and $m_{\rho''} \sim 1640$ MeV, $\Gamma_{\rho''} \sim 1290$ MeV, $\phi_{\rho\rho''} = 0^\circ$, $\sigma(\rho'' \rightarrow \omega\pi) \sim 48$ nb. The ρ' and ρ'' total width energy dependence is taken in the form

$$\Gamma_{\rho'(\rho'')} (s) = \Gamma_{\rho'(\rho'')} \frac{q_{\omega\pi}^3(s)}{q_{\omega\pi}^3(m_{\rho'(\rho'')})} \quad (32)$$

In both models the ρ meson energy dependent width has the form:

$$\Gamma_{\rho}(s) = \Gamma_{\rho^0} \frac{m_{\rho^0}^2}{s} \frac{q_{\pi\pi}^3(s)}{q_{\pi\pi}^3(m_{\rho^0})} + \frac{g_{\rho\omega\pi}^2}{12\pi} q_{\omega\pi}^3(s) \quad (33)$$

The $e^+e^- \rightarrow \omega\pi^+\pi^-$ process cross section was written in the following way:

$$\sigma_{\omega\pi\pi} = \frac{1}{s^{3/2}} \left| \sum_{i=2}^3 \frac{\Gamma_{\omega^i} m_{\omega^i}^2 \sqrt{\sigma(\omega^i \rightarrow \omega\pi^+\pi^-) m_{\omega^i}}}{D_{\omega^i}(s)} \sqrt{\frac{W_{\omega\pi\pi}(s)}{W_{\omega\pi\pi}(m_{\omega^i})}} \right|^2. \quad (34)$$

The cross sections of the $e^+e^- \rightarrow \pi^+\pi^-\pi^0$ and $\omega\pi^+\pi^-$ processes measured by SND and DM2 were fitted together. The function to be minimized was

$$\chi^2 = \chi_{3\pi(SND)}^2 + \chi_{3\pi(DM2)}^2 + \chi_{\omega\pi\pi(SND)}^2 + \chi_{\omega\pi\pi(DM2)}^2,$$

where

$$\begin{aligned} \chi_{3\pi(SND)}^2 &= \sum_s \left(\frac{\sigma_{3\pi}^{(SND)}(s) - \sigma_{3\pi}(s)}{\Delta_{3\pi}^{(SND)}(s)} \right)^2 \\ \chi_{\omega\pi\pi(SND)}^2 &= \sum_s \left(\frac{\sigma_{\omega\pi\pi}^{(SND)}(s) - \sigma_{\omega\pi\pi}(s)}{\Delta_{\omega\pi\pi}^{(SND)}(s)} \right)^2 \\ \chi_{3\pi(DM2)}^2 &= \sum_s \left(\frac{C_{3\pi} \cdot \sigma_{3\pi}^{(DM2)}(s) - \sigma_{3\pi}(s)}{\Delta_{3\pi}^{(DM2)}(s)} \right)^2 \\ \chi_{\omega\pi\pi(DM2)}^2 &= \sum_s \left(\frac{C_{\omega\pi\pi} \cdot \sigma_{\omega\pi\pi}^{(DM2)}(s) - \sigma_{\omega\pi\pi}(s)}{\Delta_{\omega\pi\pi}^{(DM2)}(s)} \right)^2 \end{aligned}$$

Here $\sigma_{3\pi(\omega\pi\pi)}^{(SND(DM2))}(s)$ are the experimental cross sections, Δ are their uncertainties, $C_{3\pi}$ and $C_{\omega\pi\pi}$ are coefficients which takes into account the relative systematic bias between SND and DM2 data. The $e^+e^- \rightarrow \pi^+\pi^-\pi^0$ cross section measured by

SND (Table II) was fitted in the energy region \sqrt{s} from 980 to 1380 MeV. The errors $\Delta_{3\pi(SND)}$ include the statistical σ_{stat} and the following systematic errors: σ_{bkg} due to inaccuracy of the background subtraction and σ_{mod} due to model dependence. Thus $\Delta_{3\pi(SND)} = \sigma_{stat} \oplus \sigma_{mod} \oplus \sigma_{bkg}$. The fitting was performed with m_{ω^i} , Γ_{ω^i} , $\sqrt{\sigma(\omega^i \rightarrow 3\pi)}$, $\sqrt{\sigma(\omega^i \rightarrow \omega\pi^+\pi^-)}$ and $\sigma(\phi \rightarrow 3\pi)$ as free parameters.

To obtain the relative bias between SND and DM2 data, the $C_{3\pi}$ and $C_{\omega\pi\pi}$ were the free parameters also. It was found that $C_{3\pi} = 1.72 \pm 0.24$, $C_{\omega\pi\pi} = 1.43 \pm 0.49$. This values does not differ within their errors and if one assumes that $C_{3\pi} = C_{\omega\pi\pi}$, then this coefficient turns out to be 1.64 ± 0.24 . SND and DM2 data actually have not have common energy points. Therefore the cross sections of the $e^+e^- \rightarrow \omega\pi^0$ process (Fig.14) measured by SND²⁶ and DM2³⁵, and cross section calculated, by using CVS hypothesis, from the CLEO2 result on the $\tau \rightarrow 3\pi\pi^0$ decay³⁶ were also studied. The $e^+e^- \rightarrow \omega\pi^0$ cross section was measured by DM2 by using $\pi^+\pi^-2\pi^0$ final state, i.e. as in the case of the $\pi^+\pi^-\pi^0$ and $\omega\pi^+\pi^-$ final states the events containing both tracks and photons were detected. This gives us a hope that all these DM2 measurements have similar systematic errors. The SND and CLEO2 data agree rather well. The DM2 and CLEO2 data points are strongly overlapped. The average ratio of the CLEO2 and DM2 cross sections is 1.54, and this agrees with $C_{3\pi} = C_{\omega\pi\pi} = 1.64 \pm 0.24$. So in further analysis the $C_{3\pi}$ and $C_{\omega\pi\pi}$ coefficients were fixed at 1.54.

The first fit was done by assuming that ω^i resonances number is equal to 3 and without taking into account $\omega\pi \rightarrow \pi^+\pi^-\pi^0$ mechanism (i.e., $\sigma_{\omega\pi \rightarrow 3\pi} = 0$ and $\sigma_{int} = 0$ were assumed). The obtained parameters of ω^i resonances are shown in Table IV. The $\sigma(\omega^1 \rightarrow 3\pi)$ differs from zero by about one standard deviation. If in this approximation one takes into account the contribution from the $\omega\pi \rightarrow \pi^+\pi^-\pi^0$ mechanism, then $\sigma(\omega^1 \rightarrow 3\pi) = 0.07 \pm^{0.32}_{0.07}$ nb, and the parameters of the ω^2 , ω^3 resonances deviate from their previous values within their statistical errors. So in the further analysis the parameter $\sigma(\omega^1 \rightarrow 3\pi)$ was fixed to zero and for the ω^2 , ω^3 resonances a more usual notation ω' , ω'' was used.

The further fittings were performed under the following assumptions:

1. the contribution from the $\omega\pi \rightarrow \pi^+\pi^-\pi^0$ was not taken into account, i.e. $\sigma_{\omega\pi \rightarrow 3\pi} = 0$, $\sigma_{int} = 0$.
2. the first model for the amplitude $A_{\omega\pi}$ was used;
3. the second model for the amplitude $A_{\omega\pi}$ was used;

The results of the fits are shown in Table V and Fig.15, 16. The obtained parameters depend weakly on the applied model.

VIII. DISCUSSION

The fit results revealed that the $e^+e^- \rightarrow \pi^+\pi^-\pi^0$ and $e^+e^- \rightarrow \omega\pi^+\pi^-$ cross sections can be described by a sum of contributions of the ω and ϕ mesons and two additional ω' , ω'' resonances. The following ω' parameters were obtained (Table V):

$$m_{\omega'} = 1500 \pm^{41}_{34} \pm 10 \text{ MeV},$$

$$\Gamma_{\omega'} = 1200 \pm^{251}_{191} \pm 25 \text{ MeV},$$

$$\sigma(\omega' \rightarrow 3\pi) = 3.43 \pm 0.46 \pm 0.08 \text{ nb},$$

$$\sigma(\omega' \rightarrow \omega\pi^+\pi^-) = 0.07 \pm^{0.08}_{0.04} \pm 0.01 \text{ nb},$$

$$\phi_{\omega\omega'} \sim 180^\circ$$

The ω' decays mostly into $\pi^+\pi^-\pi^0$: $B(\omega^2 \rightarrow 3\pi) \simeq 97\%$ and its electronic width is $\Gamma(\omega' \rightarrow e^+e^-) \simeq 650$ eV. The ω'' parameters were found to be:

$$m_{\omega''} = 1776 \pm^{33}_{27} \pm 1 \text{ MeV},$$

$$\Gamma_{\omega''} = 510 \pm^{106}_{73} \pm 7 \text{ MeV},$$

$$\sigma(\omega'' \rightarrow 3\pi) = 2.63 \pm^{0.40}_{0.37} \pm 0.13 \text{ nb},$$

$$\sigma(\omega'' \rightarrow \omega\pi^+\pi^-) = 2.56 \pm^{0.04}_{0.37} \text{ nb},$$

$$\phi_{\omega\omega''} \sim 0^\circ$$

The ω'' resonance decays with approximately equal probabilities into $\pi^+\pi^-\pi^0$ and $\omega\pi\pi$: $B(\omega'' \rightarrow 3\pi) \simeq 0.4$, $B(\omega'' \rightarrow \omega\pi\pi) \simeq 0.6$ and it has the electronic width $\Gamma(\omega'' \rightarrow e^+e^-) \simeq 700$ eV. The second errors shown are due to uncertainty of the $A_{\omega\pi}$ amplitude choice.

The obtained rather large electronic widths of the ω' and ω'' resonances may represent some challenge for the theory. In the framework of the nonrelativistic quark model one can obtain the following ratios:

$$\left| \frac{\Psi_{\omega'}^S(0)}{\Psi_\omega^S(0)} \right|^2 = \left(\frac{m_{\omega'}}{m_\omega} \right)^2 \cdot \frac{\Gamma(\omega' \rightarrow e^+e^-)}{\Gamma(\omega \rightarrow e^+e^-)} \sim 4,$$

$$\left| \frac{\Psi_{\omega''}^S(0)}{\Psi_\omega^S(0)} \right|^2 = \left(\frac{m_{\omega''}}{m_\omega} \right)^2 \cdot \frac{\Gamma(\omega'' \rightarrow e^+e^-)}{\Gamma(\omega \rightarrow e^+e^-)} \sim 6,$$

where $\Psi_V^S(0)$ is the radial wave function of the $q\bar{q}$ bound state at the origin. On the other hand, for the quark-antiquark potentials usually used to describe heavy quarkonia, such ratio are always less then unity³⁷. This is also confirmed experimentally. For example, analogous ratios for $c\bar{c}$ and $b\bar{b}$ states are: $|\Psi_{\psi(2S)}^S(0)/\Psi_{J/\psi}^S(0)|^2 \simeq 0.57$, $|\Psi_{\psi(2S)}^S(0)/\Psi_{\Upsilon(1S)}^S(0)|^2 \simeq 0.44$, $|\Psi_{\Upsilon(3S)}^S(0)/\Psi_{\Upsilon(1S)}^S(0)|^2 \simeq 0.43$. Of course the nonrelativistic quark model is unreliable for light-quark ω -states. But, surprisingly, it gives quite reasonable description of the ground state ρ , ω and ϕ mesons leptonic widths, which not radically changed in the framework of the “relativized” quark model³⁸. For comparison, the nonrelativistic quark model predictions for the two photon widths of the light pseudoscalar mesons are dramatically wrong and only “relativized” model gives reasonable result³⁹. More precise data and more deep analysis is required to draw strict conclusions, but we think that our result already is a hint that theoretical description of $\omega^{(')}$ leptonic widths is an interesting problem.

The $\sigma(\phi \rightarrow 3\pi)$ was found to be equal

$$\sigma(\phi \rightarrow 3\pi) = 647 \pm 4 \pm 37 \text{ nb}.$$

This agrees with the results of SND studies of the $e^+e^- \rightarrow \pi^+\pi^-\pi^0$ cross section in the vicinity of the ϕ resonance $\sigma(\phi \rightarrow 3\pi) = 659 \pm 35$ nb²¹. The slight deviations

in the central value and the error can be related to the difference in descriptions of the ω' , ω'' contributions used in these analysis. The fit was performed by assuming $\phi_{\omega\phi} = \Phi(s)^{30}$. If $\phi_{\omega\phi}$ is considered to be a free parameter of the fit, then its value is:

$$\phi_{\omega\phi} = 162^\circ \pm 3^\circ,$$

which agrees with $\Phi(m_\phi) = 163^\circ^{30}$.

The relative phase $\psi(s)$ between $A_{\rho\pi}$ and $A_{\omega\pi}$ amplitudes and $B(\omega \rightarrow \pi^+\pi^-)$ was obtained from the $\pi^+\pi^-$ invariant mass spectra analysis in the \sqrt{s} energy region from 1100 to 1380 MeV (Table III, Fig.17). The phase $\psi(s)$ can be also calculated from the total cross section fit results (Table V). The Fig.17 demonstrates that the phase $\psi(s)$ energy dependence cannot be described if the model with $A_{\omega\pi} = A_{\rho \rightarrow \omega\pi} + A_{\rho'' \rightarrow \omega\pi}$ is used. On the other hand, the model in which $A_{\omega\pi} = A_{\rho \rightarrow \omega\pi} + A_{\rho' \rightarrow \omega\pi} + A_{\rho'' \rightarrow \omega\pi}$ gives satisfactory description of the data. The $\omega \rightarrow \pi^+\pi^-$ decay probability was found to be:

$$B(\omega \rightarrow \pi^+\pi^-) = 2.38 \pm^{1.77}_{0.90} \pm 0.18\%$$

This result does not contradict both to OLYA measurements³¹ and world average value¹, as well as to CMD2 result³². Using the results of the total $e^+e^- \rightarrow \pi^+\pi^-\pi^0$ cross section and $\pi^+\pi^-$ invariant mass spectra analysis, the contribution of the $e^+e^- \rightarrow \rho\pi \rightarrow \pi^+\pi^-\pi^0$ mechanism to the total cross section was estimated to be $\sim 90\%$ in the energy range $\sqrt{s} = 1100 - 1380$ MeV.

For the data analysis the model which takes into account only $e^+e^- \rightarrow \rho\pi \rightarrow \pi^+\pi^-\pi^0$ and $\omega\pi^0 \rightarrow \pi^+\pi^-\pi^0$ mechanisms were used. The $e^+e^- \rightarrow \rho'^{(\prime)}\pi \rightarrow \pi^+\pi^-\pi^0$, intermediate state, as well as ρ and π mesons interaction in the final state²⁷ are also possible. Taking into account these contributions in the fit can change the $\psi(s)$ values, but the statistics collected in SND experiments is not enough for studies of such contributions. In addition, the parameters of the $\rho'^{(\prime)}$ resonances are poorly established. In the energy dependence of the total width the contributions from the following decays were not taken into account: $\omega'^{(\prime)} \rightarrow K_SK^\pm\pi^\mp, K^{*0}K^-\pi^+(\overline{K}^{*0}K^+\pi^-), K\overline{K}$, $\rho'^{(\prime)} \rightarrow \rho\pi\pi, \eta\pi^+\pi^-, K\overline{K}, K_SK^\pm\pi^\mp, K^{*0}K^-\pi^+(\overline{K}^{*0}K^+\pi^-)$. The mixing between vector mesons excitations was neglected. It is possible that more detailed model for the $A_{\omega\pi}$ and $A_{\rho\pi}$ amplitudes can change the calculated energy dependence of the phase $\psi(s)$ presented in Fig.17.

The ω' , ω'' widths obtained from the fit are rather large in comparison with their masses (this result agrees with experimental data analysis reported in⁶⁻⁸). In this context the question whether the sum of Breight-Wigner amplitudes is an adequate description of the cross sections in the energy region $m_\phi < \sqrt{s} < 2000$ MeV becomes actual.

At present in BINP (Novosibirsk) the VEPP-2000 collider with energy range from 0.36 to 2 GeV and luminosity up to $10^{32} \text{ cm}^{-2}\text{s}^{-1}$ (at $\sqrt{s} \sim 2$ GeV) is under construction⁴⁰. The two detectors SND⁴¹ and CMD-2M⁴² are upgrading for experiments at this new facility. In these experiments the increase of $e^+e^- \rightarrow \text{hadrons}$ cross sections determination accuracy is expected in the energy range $m_\phi < \sqrt{s} < 2000$ MeV. We hope, that the new data will improve the understanding of the nature of $\rho'^{(\prime)}$, $\omega'^{(\prime)}$ and $\phi'^{(\prime)}$ resonances, as well as their decay mechanisms and the theoretical methods of their description.

IX. CONCLUSION

The cross section of the process $e^+e^- \rightarrow \pi^+\pi^-\pi^0$ was measured in the SND experiment at the VEPP-2M collider in the energy region $\sqrt{s} = 980 - 1380$ MeV. The measured cross section was analyzed in the framework of the generalized vector meson dominance model together with the $e^+e^- \rightarrow \pi^+\pi^-\pi^0$ and $\omega\pi^+\pi^-$ cross sections obtained by DM2. It was found that the experimental data can be described with a sum of contributions of ω , ϕ mesons and two ω' and ω'' resonances with masses $m_{\omega'} \sim 1500$, $m_{\omega''} \sim 1770$ MeV and widths $\Gamma_{\omega'} \sim 1200$, $\Gamma_{\omega''} \sim 510$ MeV. The analysis of the dipion mass spectra in the energy region \sqrt{s} from 1100 to 1380 MeV has shown that for their description the mechanism $e^+e^- \rightarrow \omega\pi^0 \rightarrow \pi^+\pi^-\pi^0$ is required. The phase between $e^+e^- \rightarrow \omega\pi$ and $e^+e^- \rightarrow \rho\pi$ processes amplitudes was measured for the first time. Its value is close to zero and depends on energy.

ACKNOWLEDGMENTS

The authors are grateful to N.N.Achasov and A.A.Kozhevnikov for useful discussions. The present work was supported in part by grant no. 78 1999 of Russian Academy of Science for young scientists.

-
- ¹ Particle Data Group, D.E. Groom, et al., Eur.Phys.J. **C 15**, 1 (2000)
- ² A. Donnachie, Yu.S. Kalashnikova, Z.Phys. **C 59**, 621 (1993)
- ³ A. Donnachie, Yu.S. Kalashnikova, Z.Phys. **C 60**, 187 (1993)
- ⁴ A.B. Clegg, A. Donnachie Z.Phys. **C 62**, 455 (1994)
- ⁵ A. Donnachie, Yu.S. Kalashnikova, Phys. Rev. **D 60**, 114011 (1999)
- ⁶ N.N. Achasov, A.A. Kozhevnikov, Phys. Rev. **D 55**, 2663 (1997);
Yad. Fiz. **60**, 1131 (1997) [Phys. At. Nucl. **60**, 1011 (1997)]
- ⁷ N.N. Achasov, A.A. Kozhevnikov, Phys. Rev. **D 57**, 4334 (1998)
Yad. Fiz. **60**, 2212 (1997) [Phys. At. Nucl. **60**, 2029 (1997)]
- ⁸ N.N. Achasov, A.A. Kozhevnikov, Phys. Rev. **D 62**, 117503 (2000)
Yad. Fiz. **65**, 158 (2002) [Phys. At. Nucl. **65**, 155 (2002)].
- ⁹ N.N. Achasov, A.A. Kozhevnikov, and G.N. Shestakov, Phys. Lett. **50B**, 448 (1974).
N.N. Achasov, N.M. Budnev, A.A. Kozhevnikov, and G.N. Shestakov, Yad. Fiz. **23**, 610 (1976) [Sov. J. Nucl. Phys. **23**, 320 (1976)];
N.N. Achasov and G.N. Shestakov, Fiz. Elem. Chastits. At. Yadra **9**, 48 (1978)
- ¹⁰ M.N. Achasov et al., Preprint Budker INP 98-65 Novosibirsk, 1998
- ¹¹ G. Cosme et al., Nuc. Phys. **B 152**, 215 (1979)
- ¹² B. Esposito et al., Lett. Nuovo Cim. **28**, 195 (1980)
- ¹³ C. Bacci et al., Nuc. Phys. **B 184**, 31 (1981)
- ¹⁴ B. Delcourt et al., Phys. Lett **113B**, 93 (1982)
- ¹⁵ S.I. Dolinsky et al., Phys. Rep. **202**, 99 (1991)
- ¹⁶ A. Antonelli et al., Z. Phys., **C 56**, 15 (1992)
- ¹⁷ M.N. Achasov et al., Phys. Lett. **B 462**, 265 (1999)
- ¹⁸ M.N. Achasov et al., Nucl. Instr. and Meth. **A 449**, 125 (2000)
- ¹⁹ A.N. Skrinsky, in Proc. of Workshop on physics and detectors for DAΦNE, Frascati, Italy, April 4-7, 1995, p.3
- ²⁰ M.N. Achasov et al., in “Lissabon 1999 conference: Calorimetry in high energy physics”, pp. 105-120, Lisbon, Portugal, 1999.
- ²¹ M.N. Achasov et al., Phys. Rev. **D 63**, 072002 (2001)

- ²² M.N. Achasov et al., hep-ex/0106048, accepted for publication in Phys. Rev. D
- ²³ R.R. Akhmetshin et al., Phys. Lett. **B 466**, 392 (1999)
- ²⁴ K.W. Edwards et al., Phys. Rev. **D 61**, 072003 (2000)
- ²⁵ M.N. Achasov et al., Preprint, Budker INP 2001-34, Novosibirsk, 2001 (in Russian)
- ²⁶ M.N. Achasov et al., Phys. Lett. **B 486**, 29 (2000)
- ²⁷ N.N. Achasov and A.A. Kozhevnikov, Phys. Rev. D 49, 5773 (1994)
Yad. Fiz. 56, 191 (1993) [Phys. Atom. Nucl. 56, 1261 (1993)]
Int. J. Mod. Phys. A 9, 527 (1994)
- ²⁸ N.N. Achasov and A.A. Kozhevnikov, Yad. Fiz. 55, 809 (1992) [Sov. J. Nucl. Phys. 55, 449 (1992)];
Int. J. Mod. Phys. A 7, 4825 (1992).
- ²⁹ E.A. Kuraev, V.S. Fadin, Yad. Fiz. **41**, 733 (1985) [Sov. J. Nucl. Phys. **41**, 466 (1985)]
- ³⁰ N.N. Achasov, A.A. Kozhevnikov, Phys. Rev. **D 61** 054005 (2000)
Yad. Fiz. 63, 2029 (2000) [Phys. Atom. Nucl. 63, 1936 (2000)]
- ³¹ L.M. Barkov et al., Nucl. Phys. **B 256** 365 (1985)
- ³² R.R. Akhmetshin et al., hep-ex/0112031
- ³³ M.N. Achasov et al., in Proc. of Int. Workshop on e^+e^- Collisions from ϕ to J/ψ , Novosibirsk, March 1-5, 1999, Novosibirsk (2000) p.204
- ³⁴ R.R. Akhmetshin et al., Phys. Lett. **B 489**, 125 (2000)
- ³⁵ D.Bisello et al., Nucl. Phys. Proc. Suppl. 21 111 (1991)
- ³⁶ K.W. Edwards et al., Phys. Rev. **D61** 072003 (2000)
- ³⁷ C. Quigg and J.L. Rosner, Phys. Rep. **56**, 167 (1979)
- ³⁸ C.R. Munz, J. Resag, B.C. Metsch, H.R. Petry, Nucl. Phys. **A578** 418 (1994)
- ³⁹ B.C. Metsch, H.R. Petry, Acta. Phys. Polon. **B271** 3307 (1996)
- ⁴⁰ Yu.M. Shatunov et al, Project of a new electron-positron collider VEPP-2000, in Proc. of the 2000 European Particle Acc. Conf., Vienna (2000), p.439
- ⁴¹ G.N. Abramov, et al., SND Upgrade, Invited talk at “e+e- Physics at Intermediate Energies Workshop”, SLAC, Stanford, California, April 30 - May 2, 2001; e-print hep-ex/0105093
- ⁴² V.M. Aulchenko et al., Preprint Budker INP 2001-45 Novosibirsk, 2001 (in Russian)

TABLE I. Event numbers $N_{3\pi}$ of the $e^+e^- \rightarrow \pi^+\pi^-\pi^0(\gamma)$ process (after background subtraction) and N_{bkg} of background processes, integrated luminosity IL and detection efficiency $\epsilon(s, E_\gamma = 0)$, (without γ -quantum radiation. δ_{rad} is radiative correction ($\delta_{rad} = \xi(s)/\epsilon(s, E_\gamma = 0)$, $\xi(s)$ is defined through the expression (20)).

\sqrt{s} (MeV)	IL (nb $^{-1}$)	$\epsilon(s, E_\gamma = 0)$	δ_{rad}	$N_{3\pi}$	N_{bkg}
980	129	0.150	0.858	259 \pm 18	3 \pm 1
1040	69	0.153	11.706 – 131.646	90 \pm 10	4 \pm 1
1050	84	0.149	3.762 – 5.281	75 \pm 10	4 \pm 1
1060	279	0.150	1.808 – 2.018	196 \pm 16	8 \pm 2
1070	98	0.150	1.269 – 1.327	61 \pm 9	2 \pm 1
1080	578	0.150	1.060 – 1.102	325 \pm 23	22 \pm 6
1090	95	0.150	0.985 – 1.002	54 \pm 8	3 \pm 1
1100	445	0.152	0.928	255 \pm 18	14 \pm 3
1110	90	0.151	0.915	70 \pm 11	2 \pm 1
1120	306	0.150	0.889	213 \pm 17	11 \pm 3
1130	113	0.151	0.889	76 \pm 10	4 \pm 1
1140	289	0.151	0.901	177 \pm 16	9 \pm 2
1150	69	0.152	0.873	59 \pm 9	2 \pm 1
1160	320	0.152	0.877	217 \pm 17	11 \pm 2
1180	423	0.152	0.884	302 \pm 21	12 \pm 3
1190	172	0.152	0.872	125 \pm 12	4 \pm 1
1200	439	0.153	0.883	290 \pm 19	13 \pm 2
1210	151	0.153	0.871	129 \pm 12	4 \pm 1
1220	343	0.153	0.947	282 \pm 19	9 \pm 2
1230	141	0.153	0.871	103 \pm 11	4 \pm 1
1240	378	0.153	0.871	250 \pm 17	6 \pm 1
1250	209	0.154	0.871	165 \pm 14	6 \pm 1
1260	163	0.154	0.867	129 \pm 13	5 \pm 1
1270	241	0.154	0.868	175 \pm 15	8 \pm 2
1280	229	0.154	0.872	169 \pm 13	8 \pm 2
1290	272	0.155	0.866	199 \pm 15	9 \pm 2
1300	272	0.155	0.867	188 \pm 14	6 \pm 2
1310	202	0.155	0.874	153 \pm 14	5 \pm 1
1320	236	0.155	0.873	174 \pm 14	7 \pm 2
1330	293	0.156	0.876	206 \pm 15	8 \pm 2
1340	439	0.156	0.874	281 \pm 20	12 \pm 2
1350	257	0.156	0.876	169 \pm 14	6 \pm 2
1360	625	0.156	0.872	399 \pm 22	19 \pm 3
1370	256	0.156	0.879	179 \pm 15	7 \pm 2
1380	480	0.157	0.880	278 \pm 18	16 \pm 4

TABLE II. The $e^+e^- \rightarrow \pi^+\pi^-\pi^0$ cross section. \star denotes the points in which the cross section was calculated using data from Ref.²¹ (the cross section has changed only for energies $\sqrt{s} > 1027$ MeV). σ_{mod} is model uncertainty, σ_{bkg} is the error due to background subtraction, $\sigma_{eff} \oplus \sigma_{IL}$ - error due to uncertainty in detection efficiency and integrated luminosity determination (5% at the energies marked by \star and 5.4% for other energy points), $\sigma_{sys} = \sigma_{eff} \oplus \sigma_{IL} \oplus \sigma_{mod}(s) \oplus \sigma_{bkg}(s)$ is the total systematic error.

\sqrt{s} (MeV)	σ (nb)	σ_{mod} (nb)	σ_{bkg} (nb)	$\sigma_{eff} \oplus \sigma_{IL}$ (nb)	σ_{sys} (nb)
980.00	15.58 ± 1.07	0.00	0.00	0.84	0.84
984.02 \star	17.30 ± 0.80	0.00	0.00	0.86	0.86
984.21 \star	18.10 ± 0.90	0.00	0.00	0.91	0.91
1003.71 \star	37.60 ± 1.40	0.00	0.00	1.88	1.88
1003.91 \star	36.20 ± 1.30	0.00	0.00	1.81	1.81
1010.17 \star	68.50 ± 2.40	0.00	0.00	3.42	3.42
1010.34 \star	69.50 ± 2.50	0.00	0.00	3.48	3.48
1015.43 \star	220.00 ± 6.50	0.00	0.00	11.00	11.00
1015.75 \star	243.10 ± 7.50	0.00	0.00	12.16	12.16
1016.68 \star	358.90 ± 10.60	0.00	0.00	17.94	17.94
1016.78 \star	353.60 ± 11.10	0.00	0.00	17.68	17.68
1017.59 \star	493.60 ± 14.90	0.00	0.00	24.68	24.68
1017.72 \star	515.00 ± 15.30	0.00	0.00	25.75	25.75
1018.62 \star	664.20 ± 13.10	0.00	0.00	33.21	33.21
1018.78 \star	658.60 ± 11.60	0.00	0.00	32.93	32.93
1019.51 \star	667.00 ± 11.80	0.00	0.00	33.35	33.35
1019.79 \star	595.50 ± 14.10	0.00	0.00	29.77	29.77
1020.43 \star	471.20 ± 15.50	0.00	0.00	23.56	23.56
1020.65 \star	399.80 ± 14.50	0.00	0.00	19.99	19.99
1021.41 \star	270.10 ± 9.90	0.00	0.00	13.51	13.51
1021.68 \star	217.40 ± 8.50	0.00	0.00	10.87	10.87
1022.32 \star	142.90 ± 6.10	0.00	0.00	7.14	7.14
1023.27 \star	92.20 ± 3.40	0.00	0.00	4.61	4.61
1027.52 \star	15.33 ± 0.73	0.57	0.00	0.77	0.96
1028.23 \star	10.81 ± 0.62	0.52	0.00	0.54	0.75
1033.58 \star	1.75 ± 0.11	0.47	0.00	0.09	0.48
1033.84 \star	1.43 ± 0.12	0.41	0.00	0.07	0.42
1039.59 \star	0.37 ± 0.04	0.31	0.00	0.02	0.31
1039.64 \star	0.37 ± 0.03	0.31	0.00	0.02	0.31
1040.00	0.40 ± 0.04	0.33	0.00	0.02	0.33
1049.60 \star	1.12 ± 0.12	0.20	0.00	0.06	0.21
1049.81 \star	1.14 ± 0.15	0.20	0.00	0.06	0.21
1050.00	1.37 ± 0.18	0.23	0.00	0.07	0.24
1059.52 \star	1.75 ± 0.21	0.09	0.00	0.09	0.13
1059.66 \star	1.84 ± 0.28	0.09	0.00	0.09	0.13
1060.00	2.46 ± 0.20	0.14	0.00	0.13	0.19
1070.00	3.21 ± 0.47	0.07	0.04	0.17	0.19
1080.00	3.46 ± 0.24	0.07	0.09	0.19	0.22
1090.00	3.84 ± 0.57	0.03	0.07	0.21	0.22
1100.00	4.07 ± 0.29	0.00	0.09	0.22	0.24
1110.00	5.66 ± 0.89	0.00	0.05	0.31	0.31
1120.00	5.19 ± 0.42	0.00	0.11	0.28	0.30
1130.00	5.04 ± 0.67	0.00	0.10	0.27	0.29
1140.00	4.50 ± 0.40	0.00	0.09	0.24	0.26
1150.00	6.40 ± 0.98	0.00	0.10	0.35	0.36
1160.00	5.12 ± 0.39	0.00	0.10	0.28	0.29
1180.00	5.30 ± 0.37	0.00	0.09	0.29	0.30
1190.00	5.44 ± 0.53	0.00	0.08	0.29	0.30

1200.00	4.89 ± 0.32	0.00	0.09	0.26	0.28
1210.00	6.39 ± 0.60	0.00	0.08	0.34	0.35
1220.00	5.68 ± 0.41	0.00	0.07	0.31	0.32
1230.00	5.48 ± 0.59	0.00	0.09	0.30	0.31
1240.00	4.96 ± 0.34	0.00	0.04	0.27	0.27
1250.00	5.91 ± 0.51	0.00	0.08	0.32	0.33
1260.00	5.92 ± 0.60	0.00	0.10	0.32	0.33
1270.00	5.41 ± 0.47	0.00	0.10	0.29	0.31
1280.00	5.50 ± 0.43	0.00	0.10	0.30	0.31
1290.00	5.46 ± 0.42	0.00	0.10	0.29	0.31
1300.00	5.13 ± 0.40	0.00	0.07	0.28	0.29
1310.00	5.59 ± 0.52	0.00	0.07	0.30	0.31
1320.00	5.44 ± 0.44	0.00	0.09	0.29	0.31
1330.00	5.17 ± 0.38	0.00	0.08	0.28	0.29
1340.00	4.70 ± 0.34	0.00	0.08	0.25	0.27
1350.00	4.82 ± 0.41	0.00	0.07	0.26	0.27
1360.00	4.68 ± 0.27	0.00	0.09	0.25	0.27
1370.00	5.09 ± 0.43	0.00	0.08	0.27	0.29
1380.00	4.21 ± 0.28	0.00	0.09	0.23	0.25

TABLE III. The relative phase $\psi(s)$ of the amplitudes $A_{\omega\pi}$ and $A_{\rho\pi}$. N is the number of fitted histogram bins.

\sqrt{s} (MeV)	$\psi(s)$ (degree)	χ^2/N
1100	-57 \pm 56	6.5/17
1110	-66 \pm 66	13.4/17
1120	-1 \pm 43	14.6/18
1130	37 \pm 42	17.9/18
1140	130 \pm 33	10.9/18
1150	60 \pm 180	10.2/18
1160	-10 \pm 35	14.0/18
1180	25 \pm 30	6.1/18
1190	-20 \pm 53	6.2/18
1200	23 \pm 32	15.9/18
1210	131 \pm 45	5.9/20
1220	-16 \pm 51	9.0/20
1230	-102 \pm 37	8.5/20
1240	-21 \pm 45	12.1/20
1250	26 \pm 39	10.4/20
1260	-14 \pm 48	12.9/21
1270	-26 \pm 45	10.4/21
1280	1 \pm 31	12.9/21
1290	23 \pm 46	10.4/21
1300	-17 \pm 33	8.8/21
1310	32 \pm 33	14.4/22
1320	-34 \pm 54	10.8/22
1330	41 \pm 28	14.3/22
1340	30 \pm 25	9.3/22
1350	49 \pm 37	14.8/22
1360	35 \pm 23	12.1/23
1370	19 \pm 43	19.3/23
1380	23 \pm 33	9.2/23

TABLE IV. The results of the fit, taking into account three ω^i resonances.

i	m_{ω_i} , MeV	Γ_i , MeV	$\sigma(\omega^i \rightarrow 3\pi)$, nb	$\sigma(\omega^i \rightarrow \omega\pi^+\pi^-)$, nb	$\phi_{\omega\omega^i}$
1	1249 \pm 42	404 \pm 88	0.22 \pm 0.23	—	180°
2	1428 \pm 64	765 \pm 395	2.02 \pm 0.50	0.05 \pm 0.06	180°
3	1773 \pm 30	483 \pm 73	2.43 \pm 0.47	2.50 \pm 0.33	0°.

TABLE V. Fit results for the $e^+e^- \rightarrow \pi^+\pi^-\pi^0$ and $\omega\pi^+\pi^-$ cross sections. $N^{(EXP)}$ is the number of fitted points.

N	1	2	3
$\sigma(\phi \rightarrow 3\pi)$, nb	647 ± 4	646 ± 4	646 ± 4
$m_{\omega'}$, MeV	1529 ± 43	1488 ± 39	1506 ± 41
$\Gamma_{\omega'}$, MeV	1474 ± 318	1174 ± 248	1225 ± 251
$\sigma(\omega' \rightarrow 3\pi)$, nb	3.28 ± 0.45	3.35 ± 0.45	3.50 ± 0.42
$\sigma(\omega' \rightarrow \omega\pi^+\pi^-)$, nb	0.06 ± 0.06	0.06 ± 0.06	0.07 ± 0.08
$\phi_{\omega\omega'}$	180°	180°	180°
$m_{\omega''}$, MeV	1776 ± 32	1775 ± 31	1776 ± 33
$\Gamma_{\omega''}$, MeV	526 ± 80	504 ± 74	518 ± 79
$\sigma(\omega'' \rightarrow 3\pi)$, nb	2.99 ± 0.58	2.50 ± 0.50	2.76 ± 0.52
$\sigma(\omega'' \rightarrow \omega\pi^+\pi^-)$, nb	2.56 ± 0.40	2.56 ± 0.40	2.56 ± 0.40
$\phi_{\omega\omega''}$	0°	0°	0°
$\chi^2_{3\pi(SND)}/N_{3\pi}^{(SND)}$	52.2/67	49.3/67	49.7/67
$\chi^2_{3\pi(DM2)}/N_{3\pi}^{(DM2)}$	22.3/18	23.1/18	22.3/18
$\chi^2_{\omega\pi\pi(SND)}/N_{\omega\pi\pi}^{(SND)}$	5.2/9	5.4/9	5.0/9
$\chi^2_{\omega\pi\pi(DM2)}/N_{\omega\pi\pi}^{(DM2)}$	9.0/18	9.2/18	9.1/18

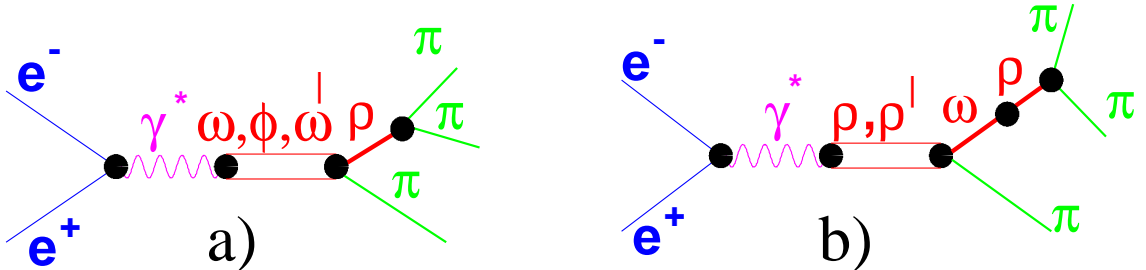


FIG. 1. The $e^+e^- \rightarrow \pi^+\pi^-\pi^0$ transition diagrams.

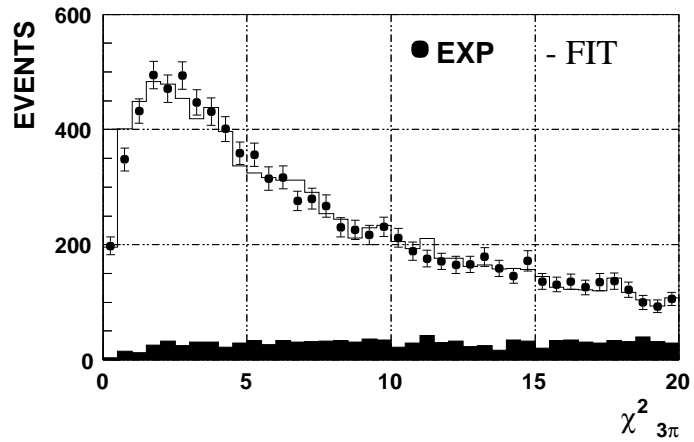


FIG. 2. The experimental $\chi^2_{3\pi}$ distribution, fitted by sum of distributions for signal and background. The background contribution is shown by dashed histogram.

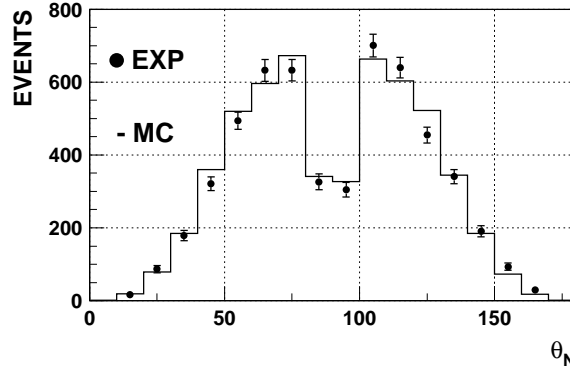


FIG. 3. The angle between the normal to the production plane and e^+e^- beam direction for $e^+e^- \rightarrow \pi^+\pi^-\pi^0$ events.

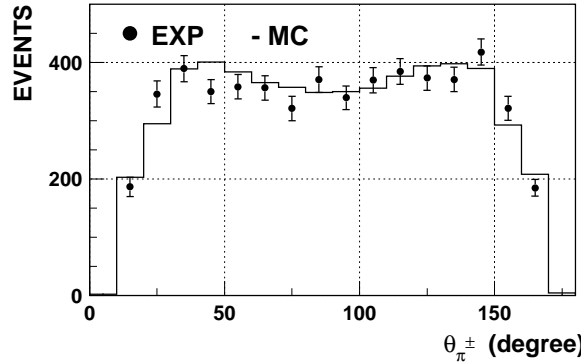


FIG. 4. The θ distribution of charged pions from the reaction $e^+e^- \rightarrow \pi^+\pi^-\pi^0$.

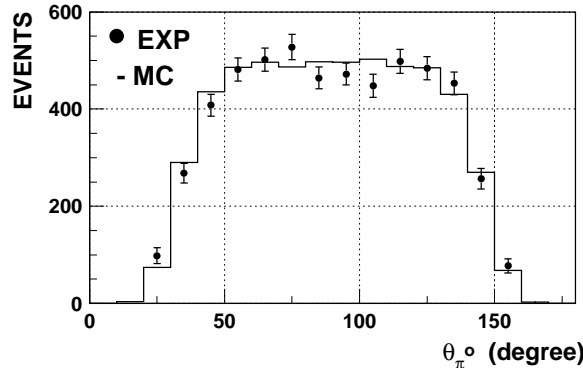


FIG. 5. The θ distribution of neutral pions from the reaction $e^+e^- \rightarrow \pi^+\pi^-\pi^0$.

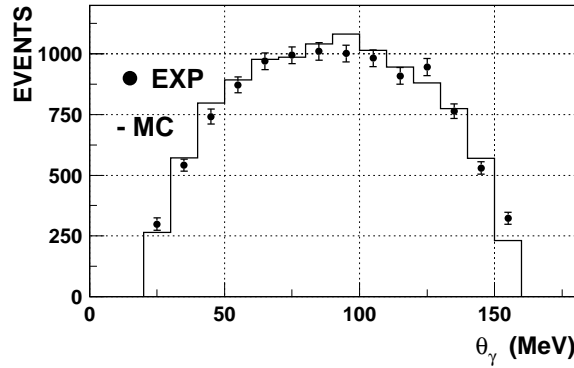


FIG. 6. The photon angular distribution.

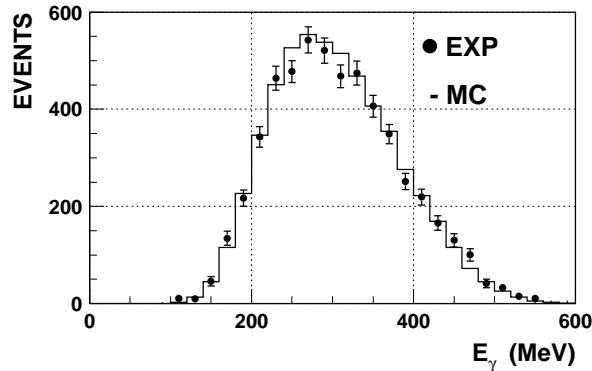


FIG. 7. The energy distribution for the most energetic photon.

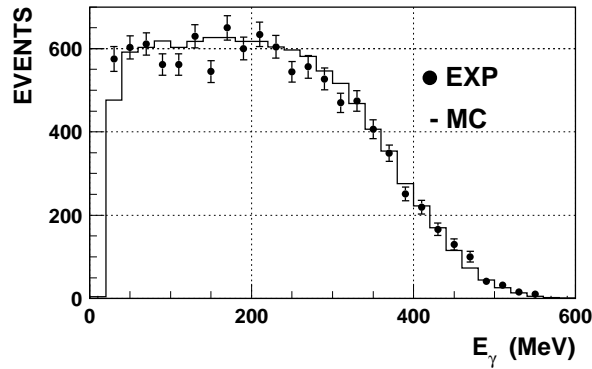


FIG. 8. Photon energy distribution.

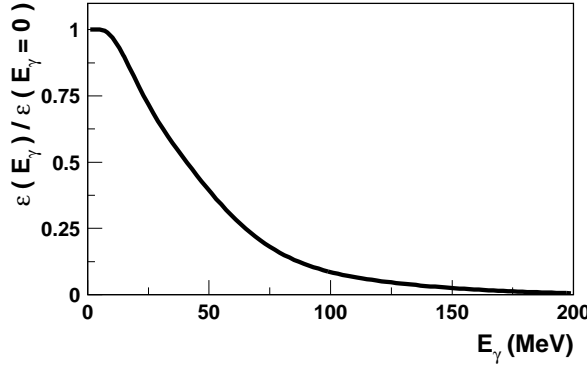


FIG. 9. The detection efficiency $\epsilon(E_\gamma)$ dependence on the radiated photon energy E_γ for $e^+e^- \rightarrow \pi^+\pi^-\pi^0(\gamma)$ events at $\sqrt{s} = 1200$ MeV, obtained by simulation.

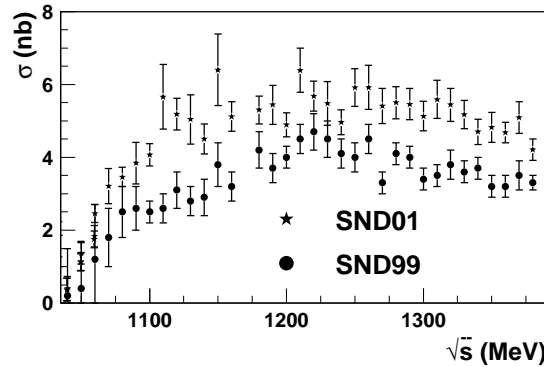


FIG. 10. Comparison of the $e^+e^- \rightarrow \pi^+\pi^-\pi^0$ cross section obtained in previous SND work¹⁷ (dots) and in this one (stars).

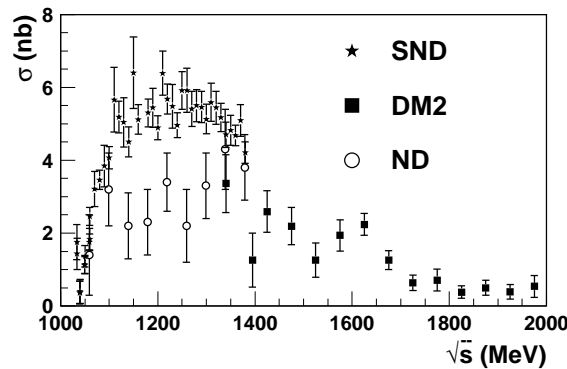


FIG. 11. The $e^+e^- \rightarrow \pi^+\pi^-\pi^0$ cross section at \sqrt{s} from 1030 to 2000 MeV. SND, ND¹⁵ and DM2¹⁶ results are shown.

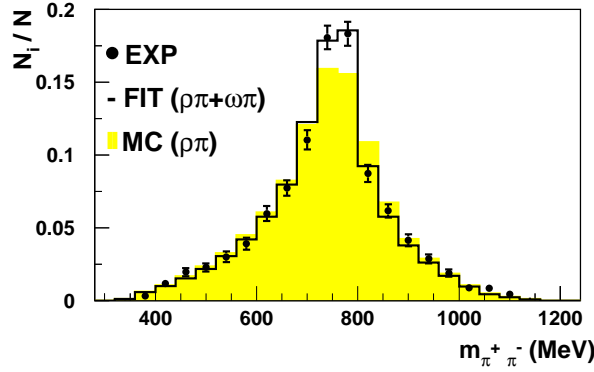


FIG. 12. The $\pi^+\pi^-$ invariant mass spectrum at \sqrt{s} from 1100 to 1380 MeV.

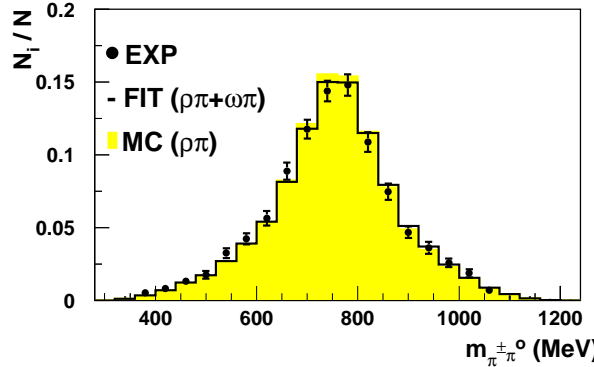


FIG. 13. The $\pi^\pm\pi^0$ invariant mass spectrum at \sqrt{s} from 1100 to 1380 MeV.

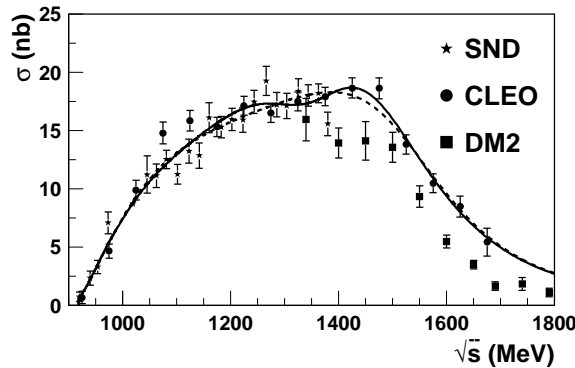


FIG. 14. The $e^+e^- \rightarrow \omega\pi$ cross section. The SND²⁶, CLEO²⁴ and DM2³⁵ data are shown. The solid curve is the cross section energy dependence in the case when $A_{\omega\pi} = A_{\rho \rightarrow \omega\pi} + A_{\rho' \rightarrow \omega\pi} + A_{\rho'' \rightarrow \omega\pi}$, dashed curve is energy dependence in the case $A_{\omega\pi} = A_{\rho \rightarrow \omega\pi} + A_{\rho'' \rightarrow \omega\pi}$.

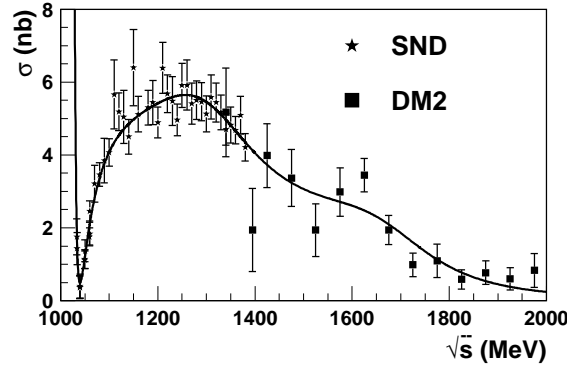


FIG. 15. The $e^+e^- \rightarrow \pi^+\pi^-\pi^0$ cross section. SND and DM2¹⁶ data are shown (the cross section measured by DM2 was increased by a factor 1.54); curve is the fit result.

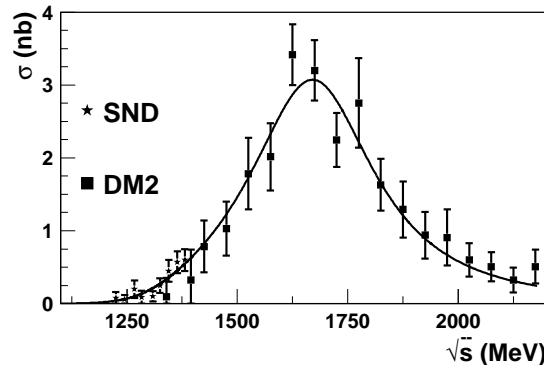


FIG. 16. The $e^+e^- \rightarrow \omega\pi^+\pi^-$ cross section. DM2¹⁶ data and preliminary SND result³³ are shown (the cross section measured by DM2 was increased by a factor 1.54); curve is the fit result.

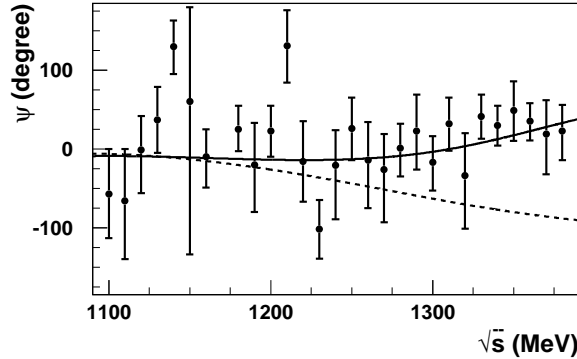


FIG. 17. The comparison of the relative phase $\psi(s)$ of the amplitudes $A_{\rho\pi}$ and $A_{\omega\pi}$ measured in this work (dots) with theoretical dependences: solid curve is the phase $\psi(s)$ in the case $A_{\omega\pi} = A_{\rho \rightarrow \omega\pi} + A_{\rho' \rightarrow \omega\pi} + A_{\rho'' \rightarrow \omega\pi}$, dashed curve is the phase $\psi(s)$ in the case $A_{\omega\pi} = A_{\rho \rightarrow \omega\pi} + A_{\rho'' \rightarrow \omega\pi}$